

Showcasing research from the Materials Science and Technology Division, Oak Ridge National Laboratory.

Unraveling luminescence mechanisms in zero-dimensional halide perovskites

First-principles calculations of exciton properties reveal the mechanisms behind the wide range of photoluminescence quantum efficiencies observed in zero-dimensional halide perovskites.

As featured in:



See Hongliang Shi,
Mao-Hua Du *et al.*,
J. Mater. Chem. C, 2018, 6, 6398.



rsc.li/materials-c

Registered charity number: 207890



Cite this: *J. Mater. Chem. C*, 2018,
6, 6398

Unraveling luminescence mechanisms in zero-dimensional halide perovskites†‡

Dan Han,^a Hongliang Shi,^a Wenmei Ming,^c Chenkun Zhou,^e Biwu Ma,^e Bayrammurad Saparov,^f Ying-Zhong Ma,^c Shiyu Chen^b and Mao-Hua Du^{*c}

Zero-dimensional (0D) halides perovskites, in which anionic metal-halide octahedra (MX₆)^{4−} are separated by organic or inorganic counteranions, have recently shown promise as excellent luminescent materials. However, the origin of the photoluminescence (PL) and, in particular, the different photophysical properties in hybrid organic–inorganic and all inorganic halides are still poorly understood. In this work, first-principles calculations were performed to study the excitons and intrinsic defects in 0D hybrid organic–inorganic halides (C₄N₂H₁₄X)₄SnX₆ (X = Br, I), which exhibit a high photoluminescence quantum efficiency (PLQE) at room temperature (RT), and also in the 0D inorganic halide Cs₄PbBr₆, which suffers from strong thermal quenching when *T* > 100 K. We show that the excitons in all three 0D halides are strongly bound and cannot be detrapped or dissociated at RT, which leads to immobile excitons in (C₄N₂H₁₄X)₄SnX₆. However, the excitons in Cs₄PbBr₆ can still migrate by tunneling, enabled by the resonant transfer of excitation energy (Dexter energy transfer). The exciton migration in Cs₄PbBr₆ leads to a higher probability of trapping and nonradiative recombination at the intrinsic defects. We show that a large Stokes shift and the negligible electronic coupling between luminescent centers are important for suppressing exciton migration; thereby, enhancing the photoluminescence quantum efficiency. Our results also suggest that the frequently observed bright green emission in Cs₄PbBr₆ is not due to the exciton or defect-induced emission in Cs₄PbBr₆ but rather the result of exciton emission from CsPbBr₃ inclusions trapped in Cs₄PbBr₆.

Received 17th March 2018,
Accepted 9th May 2018

DOI: 10.1039/c8tc01291a

rsc.li/materials-c

1. Introduction

Hybrid organic–inorganic metal halides (HOIMHs) are a large family of materials that consist of 3D, 2D, 1D, or 0D anionic

metal halide frameworks and organic cations.¹ The broad compositional and structural flexibilities of HOIMHs offer great tunability of their physical properties, which have been explored for a wide range of applications, such as photovoltaics,^{2–5} light-emitting diode (LED),⁶ laser,^{6,7} radiation detection,⁸ and down-converting phosphors.^{9–15} Pb and Sn based 3D halide perovskites exhibit excellent carrier transport properties.^{16–19} CH₃NH₃PbI₃ and related materials have been extensively studied as solar absorber materials.^{2–5} Lowering the dimensionality of the poly-anionic inorganic networks from 3D, 2D, 1D, to 0D leads to increasingly more localized electronic states and consequently narrower conduction and valence bands, which promote the self-trapping of excitons and stronger exciton emission. As a result, efficient luminescence at a wide range of emission wavelengths has been observed in low-dimensional HOIMHs;^{9–15,20,21} the highest PLQE were found in 0D compounds.^{15,22} The high attainable PLQE and the tunable emission energy render the 0D metal halides promising luminescent materials for energy-efficient lighting and radiation detection.

Recently, Ma and coworkers reported a series of visible-light-emitting 0D HOIMHs (C₄N₂H₁₄X)₄SnX₆ (X = Br, I) with high PLQE [up to unity for (C₄N₂H₁₄Br)₄SnBr₆ and 80% for (C₄N₂H₁₄I)₄SnI₆]; the highly efficient luminescence was attributed to self-trapped excitons.¹⁵ In addition, a related 0D inorganic metal halide

^a Key Laboratory of Polar Materials and Devices (Ministry of Education), East China Normal University, Shanghai 200241, China

^b Department of Physics, East China Normal University, Shanghai 200241, China

^c Materials Science and Technology Division, Oak Ridge National Laboratory, Oak Ridge, TN 37831, USA. E-mail: mhdu@ornl.gov

^d Key Laboratory of Micro-Nano Measurement-Manipulation and Physics (Ministry of Education), Department of Physics, Beihang University, Beijing 100191, China. E-mail: hlshi@buaa.edu.cn

^e Department of Chemical and Biomedical Engineering, FAMU-FSU College of Engineering, Tallahassee, FL 32310, USA

^f Department of Chemistry and Biochemistry, University of Oklahoma, 101 Stephenson Parkway, Norman, OK 73019, USA

† This manuscript has been authored by UT-Battelle, LLC under Contract No. DE-AC05-00OR22725 with the U.S. Department of Energy. The United States Government retains and the publisher, by accepting the article for publication, acknowledges that the United States Government retains a non-exclusive, paid-up, irrevocable, world-wide license to publish or reproduce the published form of this manuscript, or allow others to do so, for United States Government purposes. The Department of Energy will provide public access to these results of federally sponsored research in accordance with the DOE Public Access Plan (<http://energy.gov/downloads/oe-public-access-plan>).

‡ Electronic supplementary information (ESI) available. See DOI: 10.1039/c8tc01291a

§ Both authors contributed equally to this work.

Cs_4PbBr_6 , which has the same 4-1-6 composition ratio as the highly luminescent $(\text{C}_4\text{N}_2\text{H}_{14}\text{X})_4\text{SnX}_6$ ($\text{X} = \text{Br}, \text{I}$), has been reported to display strong green luminescence (~ 520 nm) with a high PLQE up to 97%.^{23–29} However, the origin of the green luminescence in Cs_4PbBr_6 has been under intense debate.^{27,29–33} Several luminescence mechanisms have been proposed, such as exciton or defect-related emission in Cs_4PbBr_6 and emission by CsPbBr_3 impurities.³³ Despite the strong green emission reported by many authors,^{23–28} Akkerman *et al.* showed no significant visible light emission from Cs_4PbBr_6 ³⁰ and Nikl *et al.*, showed that bulk Cs_4PbBr_6 exhibits UV emission (centered at 375 nm), which suffers from severe reduction of PL intensity when $T > 100$ K;³⁴ however, the mechanism of the thermal quenching of luminescence is unknown. The lack of a microscopic understanding of the underlying mechanisms behind various photo-physical properties observed in 0D HOIMHs and related inorganic metal halides hindered the design and the development of these novel materials towards high PLQE and optimized the emission energies for targeted applications.

In this work, hybrid density functional theory (DFT) calculations were performed to study the electronic and dielectric properties, exciton dynamics (optical excitation, relaxation, and emission), and exciton trapping by defects in 0D HOIMHs, *i.e.*, $(\text{C}_4\text{N}_2\text{H}_{14}\text{X})_4\text{SnX}_6$ ($\text{X} = \text{Br}, \text{I}$) and the related inorganic Cs_4PbBr_6 . The calculated optical excitation and emission energies of excitons in $(\text{C}_4\text{N}_2\text{H}_{14}\text{X})_4\text{SnX}_6$ ($\text{X} = \text{Br}, \text{I}$) and Cs_4PbBr_6 are in excellent agreement with the experimental results, demonstrating the validity of the hybrid DFT method in describing both the electronic structure and the structural relaxation at the excited state of these 0D metal halides. Our results show that excitons are immobile in $(\text{C}_4\text{N}_2\text{H}_{14}\text{Br})_4\text{SnBr}_6$ ($\text{X} = \text{Br}, \text{I}$) but can migrate in Cs_4PbBr_6 by tunneling enabled by resonant transfer of excitation energy. The counteranions play a critical role in determining the efficiency of exciton migration and the subsequent trapping at halogen vacancies, which explains the high PLQE in $(\text{C}_4\text{N}_2\text{H}_{14}\text{X})_4\text{SnX}_6$ and the strong thermal quenching in Cs_4PbBr_6 . Furthermore, we show that the frequently observed green emission in Cs_4PbBr_6 is not due to the intrinsic properties of Cs_4PbBr_6 but rather the result of CsPbBr_3 inclusion.

II. Computational methods

Electronic band structures, density of states (DOS), and dielectric constants of bulk compounds were calculated using Perdew–Burke–Ernzerhof (PBE) exchange–correlation functional³⁵ while excitons and defects were treated by using the more advanced hybrid PBE0 functional,³⁶ which has 25% non-local Fock exchange. Previous PBE0 calculations have provided accurate results in exciton excitation and emission energies in hybrid organic–inorganic halide perovskites.³⁷ Spin–orbit coupling (SOC) was included in the calculations on Cs_4PbBr_6 only because it was shown previously that the SOC has a strong effect on Pb-6p levels.³⁸ Our tests show that including the SOC reduces the band gaps of $(\text{C}_4\text{N}_2\text{H}_{14}\text{Br})_4\text{SnBr}_6$, $(\text{C}_4\text{N}_2\text{H}_{14}\text{I})_4\text{SnI}_6$, and Cs_4PbBr_6 , by 0.11 eV, 0.18 eV, and 0.69 eV, respectively.

(More details of the computational methods are given in Section S1 in the ESI.†)

Following the Franck–Condon principle, the exciton excitation and emission energies were obtained by calculating the total energy differences between the excited and the ground states using the PBE0-optimized ground-state and excited-state structures, respectively. For $(\text{C}_4\text{N}_2\text{H}_{14}\text{X})_4\text{SnX}_6$ ($\text{X} = \text{Br}, \text{I}$), a spin-singlet exciton was considered when calculating the excitation energy because this is a spin-allowed transition while a spin-triplet exciton was considered for calculating the emission energy because the spin-triplet exciton is more stable than the spin-singlet one. The slow PL decay on the order of microseconds observed for $(\text{C}_4\text{N}_2\text{H}_{14}\text{X})_4\text{SnX}_6$ ($\text{X} = \text{Br}, \text{I}$)¹⁵ is consistent with the spin-forbidden transition for the radiative recombination of the spin-triplet excitons. For Cs_4PbBr_6 , there is strong mixing between the spin-singlet and -triplet states of the exciton due to the strong SOC effect on Pb; thus, the SOC was included in calculations. The exciton binding energy (relative to a free exciton) was calculated by $\Delta E_b = E(\text{GS}) + E_g - E(\text{exciton})$, where $E(\text{GS})$ and $E(\text{exciton})$ are the total energies of the ground state and the exciton, respectively, and E_g is the band gap.

III. Results and discussion

A. Electronic structure

$(\text{C}_4\text{N}_2\text{H}_{14}\text{X})_4\text{SnX}_6$ ($\text{X} = \text{Br}, \text{I}$) and Cs_4PbBr_6 all have the 0D structure that contains isolated anionic metal-halide octahedra $(\text{MX}_6)^{4-}$ separated by $(\text{C}_4\text{N}_2\text{H}_{14}\text{X})^+$ or Cs^+ counteranions (Fig. 1); in addition, they have the same 4-1-6 composition ratio. The valence and the conduction bands of all three compounds are dominated by the electronic states derived from anionic $(\text{MX}_6)^{4-}$ clusters as shown by the DOS in Fig. 2. The electronic bands derived from the counteranions are far away from the band gap. The band structure of Cs_4PbBr_6 in Fig. 2(e) is in good agreement with previous PBE calculations.³⁹ The PBE0 band gaps of $(\text{C}_4\text{N}_2\text{H}_{14}\text{X})_4\text{SnX}_6$ ($\text{X} = \text{Br}, \text{I}$) and Cs_4PbBr_6 are 5.1 eV, 4.43 eV, and 4.80 eV, respectively. (The PBE³⁵ and PBE0³⁶ band gaps are compared in the Section S2 in the ESI.†) Both the conduction and the valence bands of $(\text{C}_4\text{N}_2\text{H}_{14}\text{X})_4\text{SnX}_6$ are nearly dispersionless [Fig. 2(a) and (c)], indicating negligible electronic coupling between SnX_6 clusters. The shortest inter-cluster Br–Br distance in $(\text{C}_4\text{N}_2\text{H}_{14}\text{Br})_4\text{SnBr}_6$ is 6.33 Å. On the other hand, the shortest inter-cluster Br–Br distance in Cs_4PbBr_6 is only 4.07 Å (due to the relatively small Cs^+ ion), which leads to inter-cluster wavefunction overlap and the relatively dispersive valence band as shown in Fig. 2(e). (This has an important consequence on exciton migration, which is to be discussed in Section IIID).

B. Exciton binding, relaxation, excitation, and emission

The small dispersion in both the valence and the conduction bands of $(\text{C}_4\text{N}_2\text{H}_{14}\text{X})_4\text{SnX}_6$ ($\text{X} = \text{Br}, \text{I}$) and Cs_4PbBr_6 as shown in Fig. 2 promote strong localization of excitons at the $(\text{MX}_6)^{4-}$ metal halide octahedra. The calculated binding energies of the relaxed excitons (relative to free excitons) (E_b^{relax} in Table 1) in $(\text{C}_4\text{N}_2\text{H}_{14}\text{Br})_4\text{SnBr}_6$, $(\text{C}_4\text{N}_2\text{H}_{14}\text{I})_4\text{SnI}_6$, and Cs_4PbBr_6 are 2.19 eV,

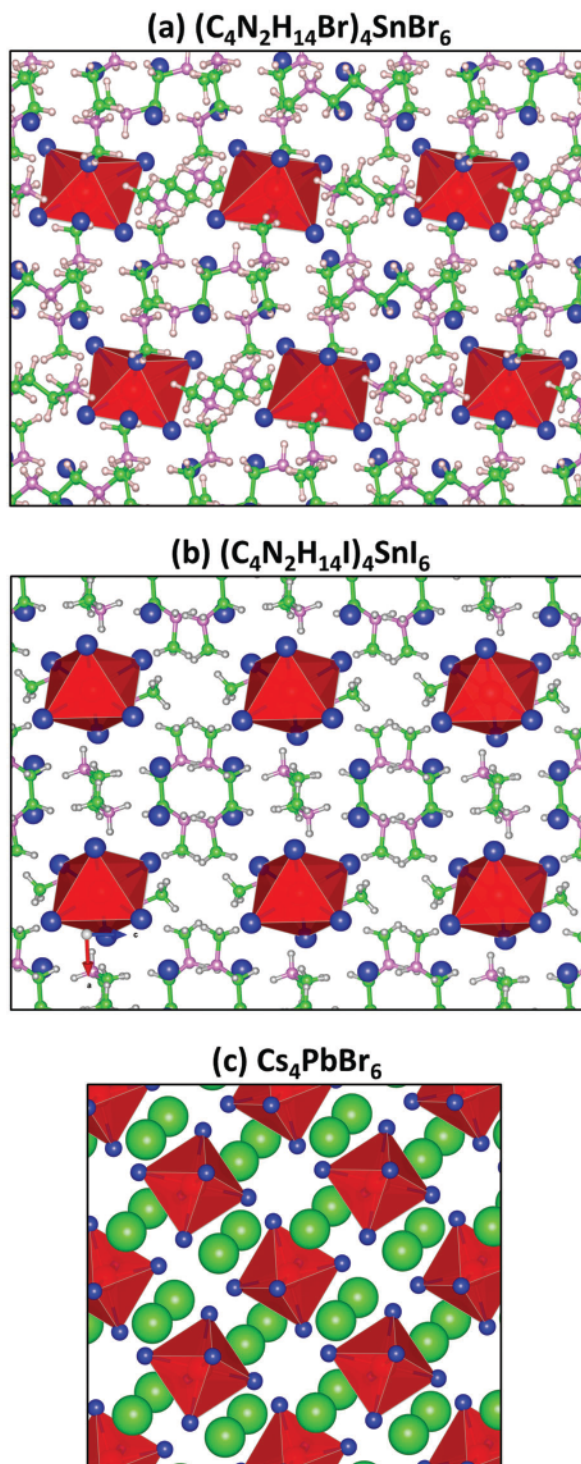


Fig. 1 Structures of (a) $(\text{C}_4\text{N}_2\text{H}_{14}\text{Br})_4\text{SnBr}_6$, (b) $(\text{C}_4\text{N}_2\text{H}_{14}\text{I})_4\text{SnI}_6$, and (c) Cs_4PbBr_6 .

1.93 eV, and 1.25 eV, respectively. The large exciton binding energies suggest that free excitons do not exist in these 0D halide perovskites in the entire temperature range where these compounds are stable as solids. The electron–hole Coulomb attraction is strong as indicated by the large binding energies (> 1 eV) of unrelaxed excitons ($E_{\text{B}}^{\text{unrelax}}$ in Table 1). Such a strong Coulomb binding is due to the 0D crystal structure, which not

only confines the electron and the hole within a metal-halide octahedron but also reduces the dielectric constant substantially from the 3D compounds. The calculated static dielectric constants of $(\text{C}_4\text{N}_2\text{H}_{14}\text{Br})_4\text{SnBr}_6$, $(\text{C}_4\text{N}_2\text{H}_{14}\text{I})_4\text{SnI}_6$, and Cs_4PbBr_6 are 11.9, 7.7, and 7.7, respectively, much smaller than those of the 3D halide perovskite counterparts (e.g., 32.0 in $\text{CH}_3\text{NH}_3\text{SnBr}_3$, 29.5 in $\text{CH}_3\text{NH}_3\text{SnI}_3$, 19.2 in CsSnBr_3). The large ionic contribution to the static dielectric constant commonly seen in halides that contain ns^2 cations (e.g., Sn^{2+} , Pb^{2+})^{40–42} is suppressed by the 0D crystal structure. [See ESI† (Section S3) for details.] Besides the strong Coulomb binding, the extended excited-state structural relaxation (as evidenced by significant bond length changes shown in Table 1) lowers the exciton energies substantially in $(\text{C}_4\text{N}_2\text{H}_{14}\text{X})_4\text{SnX}_6$ (X = Br, I), i.e., 0.97 eV and 0.75 eV, respectively (Table 1). However, the excited-state structural relaxation lowers the total energy by only 0.08 eV in Cs_4PbBr_6 . The calculated exciton relaxation energy and the exciton emission energy in Cs_4PbBr_6 are in good agreement with a recent theoretical study.⁴³ Thus, the excited-state potential energy landscape for Cs_4PbBr_6 is much flatter than those for $(\text{C}_4\text{N}_2\text{H}_{14}\text{X})_4\text{SnX}_6$ (X = Br, I) [Fig. S1, ESI†].

Here, we use $(\text{C}_4\text{N}_2\text{H}_{14}\text{Br})_4\text{SnBr}_6$ as an example to show the details of exciton dynamics revealed by our calculations. Upon excitation of one electron, the unrelaxed spin-singlet exciton is localized on only one $(\text{SnBr}_6)^{4-}$ cluster and inserts deep electron and the hole levels inside the band gap [Fig. S2(a), ESI†]. The spin-singlet exciton undergoes the intersystem crossing and becomes a more stable spin-triplet exciton. Our calculations show that the spin-triplet exciton is more stable than the spin-singlet exciton by 0.28 eV without structural relaxation. The structural relaxation of both the spin-triplet and singlet excitons increases the triplet–singlet energy splitting to 0.33 eV. This is supported by the observed slow emission decay (on the order of μs),¹⁵ which is characteristic for the spin-forbidden triplet exciton emission. Since only one of the three Sn-5p orbitals is occupied by the excited electron, the structure relaxation of the spin-triplet exciton causes the elongation of two Sn–Br bonds within the $(\text{SnBr}_6)^{4-}$ octahedron; the other four Sn–Br bonds are shortened due to the hole centered at Sn, which attracts the four Br^- ions. Thus, the electron state is a Sn-5p–Br-4p-hybridized orbital while the hole state is a Sn-5s–Br-4p-hybridized orbital and both are of antibonding character. These are demonstrated by the calculated partial density contours of the electron and the hole wavefunctions in the relaxed spin-triplet exciton (Fig. 3). The exciton relaxation enhances localization as both the electron and the hole levels are moved deeper into the band gap as shown in the DOS (Fig. S2, ESI†). The two Sn–Br bonds where the excited electron resides are elongated by 19.8% in average while the four Sn–Br bonds where the hole resides are shortened by 9.9% in average. In $(\text{C}_4\text{N}_2\text{H}_{14}\text{I})_4\text{SnI}_6$ and Cs_4PbBr_6 , a similar structural distortion occurs upon exciton excitation as shown in Table 1. We also tested a different exciton structure, in which the hole is localized by forming a halogen–halogen bond like a V_{k} center.⁴⁴ However, such an exciton structure is not stable in all three compounds. Table 2 shows the calculated exciton excitation and emission

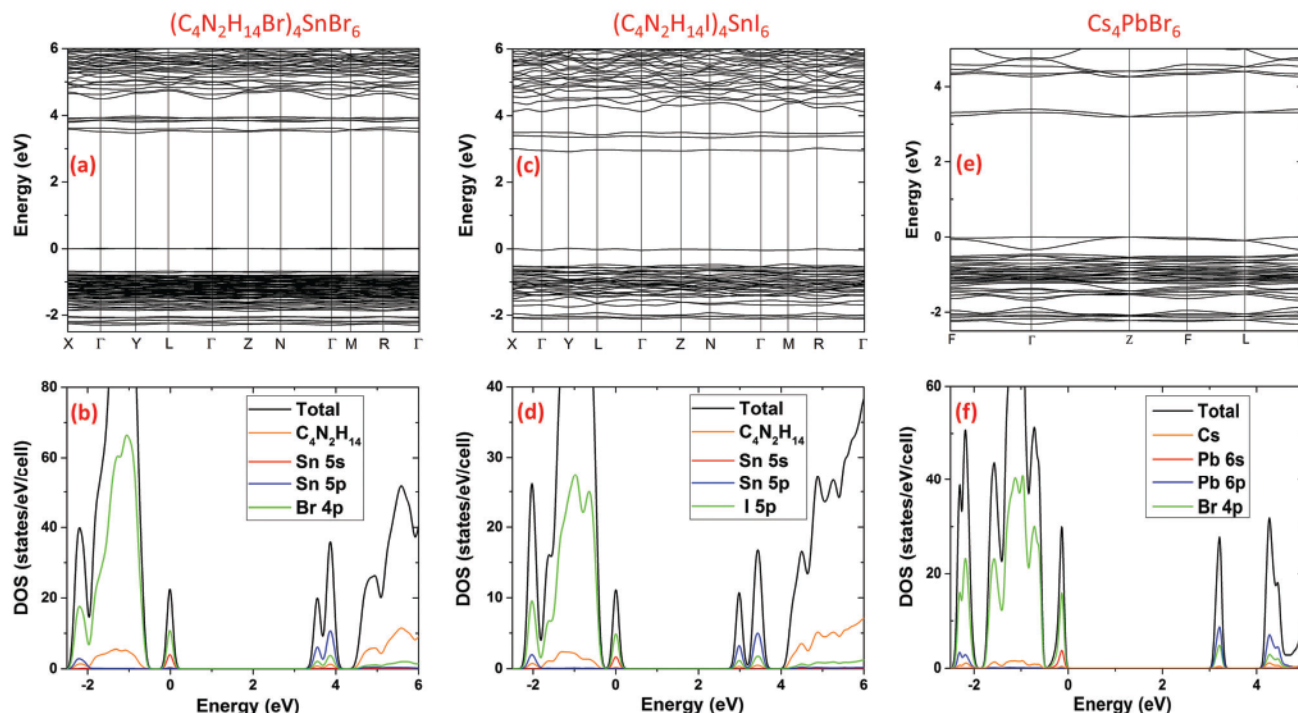


Fig. 2 Electronic band structures and density of states (DOS) of $(\text{C}_4\text{N}_2\text{H}_{14}\text{Br})_4\text{SnBr}_6$ (a and b), $(\text{C}_4\text{N}_2\text{H}_{14}\text{I})_4\text{SnI}_6$ (c and d), and Cs_4PbBr_6 (e and f) calculated using PBE functionals. The spin-orbit coupling (SOC) is included in the calculations for Cs_4PbBr_6 due to the strong effect of the SOC on Pb-6p levels. Note that the PBE band gaps are underestimated.

Table 1 Binding energies of the unrelaxed ($E_{\text{B}}^{\text{unrelax}}$) and the relaxed ($E_{\text{B}}^{\text{relax}}$) excitons, exciton relaxation energies ($\Delta E = E_{\text{B}}^{\text{relax}} - E_{\text{B}}^{\text{unrelax}}$), and the structural distortion of the metal halide octahedron (MX_6^{4-}) due to the exciton relaxation: average increase (decrease) of the length of the two (four) metal-halogen (M-X) bonds where the electron (hole) resides within the $(\text{MX}_6)^{4-}$ cluster. All the results are based on hybrid functional PBE0 calculations

	$(\text{C}_4\text{N}_2\text{H}_{14}\text{Br})_4\text{SnBr}_6$	$(\text{C}_4\text{N}_2\text{H}_{14}\text{I})_4\text{SnI}_6$	Cs_4PbBr_6
$E_{\text{B}}^{\text{unrelax}}$ (eV)	1.22	1.18	1.17
$E_{\text{B}}^{\text{relax}}$ (eV)	2.19	1.93	1.25
ΔE (eV)	0.97	0.75	0.08
Two elongated M-X bonds	19.8%	17.0%	15.6%
Four shortened M-X bonds	-9.9%	-6.5%	-3.7%

energies in $(\text{C}_4\text{N}_2\text{H}_{14}\text{X})_4\text{SnX}_6$ ($\text{X} = \text{Br}, \text{I}$) and Cs_4PbBr_6 ; the excellent agreement between theory and experiment demonstrates that the electron-hole Coulomb binding in the exciton and the excited-state structural relaxation are described very well by the PBE0 calculation.

C. Exciton trapping at halogen vacancies

Photoexcited excitons can be trapped by native defects and undergo nonradiative recombination; thereby, causing loss of photon emission. The dominant native defects in halides are usually vacancies.^{46,47} Among vacancies, the halogen vacancies are known to be deep centers in halides. However, the halogen vacancies in several 3D halide perovskites (such as $\text{CH}_3\text{NH}_3\text{PbI}_3$ and CsPbBr_3) were found to be shallow.^{42,48,49} To clarify this issue in 0D metal halides, we calculated the exciton

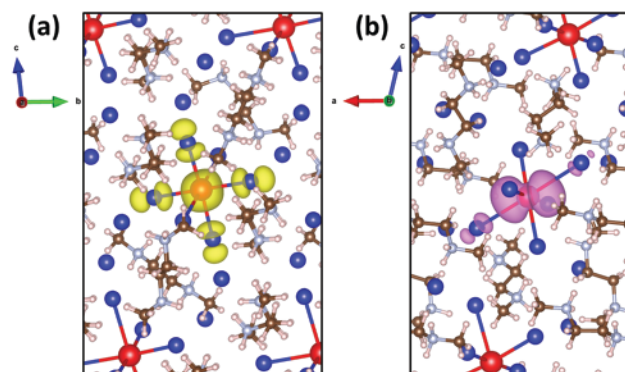


Fig. 3 Partial density contours of the hole (a) and the electron (b) in a relaxed exciton in $(\text{C}_4\text{N}_2\text{H}_{14}\text{Br})_4\text{SnBr}_6$; (a) and (b) are viewed from the directions of axes a and b , respectively.

trapping energies at the most stable V_X^+ in $(\text{C}_4\text{N}_2\text{H}_{14}\text{Br})_4\text{SnBr}_6$, $(\text{C}_4\text{N}_2\text{H}_{14}\text{I})_4\text{SnI}_6$, and Cs_4PbBr_6 ; they were found to be 0.41 eV, 0.22 eV, and 0.59 eV (Table 3), respectively, indicating deep trapping. [See the ESI† (Section S4) for details of the structure and the electronic structure of the bound excitons at halogen vacancies.] Thus, these halogen vacancies are effective exciton traps, which are abundant in solution-grown halide perovskites, and may cause nonradiative recombination of excitons. However, if the excitons are immobile, the probability of excitons getting trapped by halogen vacancies and other defects would be significantly reduced. Thus, the mobility of excitons is the key to the efficiency of the non-radiative recombination at defects.

Table 2 Exciton excitation and emission energies as well as Stoke shifts in $(\text{C}_4\text{N}_2\text{H}_{14}\text{Br})_4\text{SnBr}_6$, $(\text{C}_4\text{N}_2\text{H}_{14}\text{I})_4\text{SnI}_6$, and Cs_4PbBr_6 , calculated using hybrid PBE0 functionals. The experimentally measured excitation and emission energies are shown in parentheses

	Excitation energy (eV)	Emission energy (eV)	Stokes shift (eV)
$(\text{C}_4\text{N}_2\text{H}_{14}\text{Br})_4\text{SnBr}_6$	3.88 (3.49 ^a)	2.15 (2.34 ^a)	1.73 (1.15 ^a)
$(\text{C}_4\text{N}_2\text{H}_{14}\text{I})_4\text{SnI}_6$	3.25 (3.03 ^a)	1.93 (1.98 ^a)	1.32 (1.05 ^a)
Cs_4PbBr_6	3.63 (4.00; ^b 3.95 ^{c,d})	3.05 (3.31 ^b)	0.58 (0.69 ^b)

^a Ref. 15. ^b Ref. 34. ^c Ref. 30. ^d Ref. 45.

D. Exciton migration by resonant energy transfer and thermal quenching of luminescence in Cs_4PbBr_6

The exciton diffusion by thermal activation should be inefficient in $(\text{C}_4\text{N}_2\text{H}_{14}\text{X})_4\text{SnX}_6$ (X = Br, I) and Cs_4PbBr_6 at room temperature due to the large exciton binding energies (Table 1) and the weak inter-cluster electronic and vibrational coupling. Exciton tunneling between inorganic clusters should be more efficient if the resonant condition is satisfied, *i.e.*, there is a spectral overlap between exciton excitation and emission and significant interaction between MX_6 clusters through wavefunction overlap or multipolar interaction.^{50,51} Clearly, a large Stokes shift is critically important for suppressing the resonant transfer of excitation energy in 0D halide perovskites as discussed below.

Stronger excited-state structural relaxation leads to a larger Stokes shift as shown in Tables 1 and 2. The volumes for one formula unit of $(\text{C}_4\text{N}_2\text{H}_{14}\text{Br})_4\text{SnBr}_6$, $(\text{C}_4\text{N}_2\text{H}_{14}\text{I})_4\text{SnI}_6$, and Cs_4PbBr_6 are 974.945 Å³, 1124.94 Å³, and 470.585 Å³, respectively. Clearly, among these three 0D compounds, Cs_4PbBr_6 has the most compact structure [Fig. 1(c)], which results in the smallest exciton relaxation energy (Table 1) and the smallest Stokes shift (Table 2) (see a schematic in Fig. S1, ESI†). The experimentally measured exciton excitation and the emission energies in Cs_4PbBr_6 are 4.00 eV (310 nm) and 3.31 eV (375 nm), respectively. The Stokes shift of 65 nm is relatively small compared to the typical broad exciton emission bands (FWHM > 100 nm) observed in 0D metal halides.¹⁵ At 4.2 K, the exciton excitation and emission bands in Cs_4PbBr_6 do not overlap and the UV emission at 375 nm was observed.³⁴ With increasing temperature, both the excitation and the emission bands are expected to be broadened due to the phonon participation in the optical transitions. The phonon broadening should be significant in low-dimensional metal halides due to the soft phonons involved.³² For example, as temperature rises from 77 K to RT, the FWHM of the exciton emission band increases from 63 nm (0.276 eV) to 105 nm

(0.409 eV) for $(\text{C}_4\text{N}_2\text{H}_{14}\text{Br})_4\text{SnBr}_6$ and from 63 nm (0.198 eV) to 118 nm (0.373 eV) for $(\text{C}_4\text{N}_2\text{H}_{14}\text{I})_4\text{SnI}_6$.¹⁵ The exciton emission band for Pb compounds appear to be even broader than those in the Sn compounds shown above. For 1D $\text{C}_4\text{N}_2\text{H}_{14}\text{PbBr}_4$, the FWHM of the emission band due to the self-trapped exciton (STE) is already broad at 77 K, *i.e.*, 103 nm (0.455 eV);¹⁴ at RT, the FWHM is estimated to be about 149 nm (0.836 eV). The exciton excitation band for the low-dimensional metal halides is also broad at RT. For example, the FWHM of the exciton excitation bands in $(\text{C}_4\text{N}_2\text{H}_{14}\text{Br})_4\text{SnBr}_6$ and $(\text{C}_4\text{N}_2\text{H}_{14}\text{I})_4\text{SnI}_6$ at RT are 81 nm (0.896 eV) and 116 nm (0.979 eV), respectively. Based on the above results, it is expected that the excitation and the emission bands of excitons in Cs_4PbBr_6 are both broadened with increasing temperature and overlap at RT due to the relatively small Stokes shift of 65 nm (0.69 eV). This is supported by the observed broad and overlapping excitonic absorption and emission bands in the UV region in the optical absorption and PL spectra in Cs_4PbBr_6 .³² The spectral overlap and the significant electronic coupling among $(\text{PbBr}_6)^{4-}$ octahedra in Cs_4PbBr_6 [evidenced by the relatively dispersive valence band [Fig. 2(e)] should enable nonradiative resonant transfer of the excitation energy (Dexter energy transfer⁵¹), which leads to exciton migration (Fig. 4)].^{50,51} Thus, the mechanism of thermal quenching of the UV emission (when $T > 100$ K) in Cs_4PbBr_6 ³⁴ is likely the concentration quenching (rather than the exciton dissociation), which is frequently observed in heavily activator-doped phosphors,⁵⁰ *i.e.*, the high concentration of luminescent centers with a spectral overlap between excitation and emission enables resonant transfer of excitation energy among luminescent centers and the subsequent energy loss at defects. The role of the rising temperature is to increase the spectral overlap.

E. Immobile excitons and high PLQE in $(\text{C}_4\text{N}_2\text{H}_{14}\text{X})_4\text{SnX}_6$ (X = Br, I)

In contrast to Cs_4PbBr_6 , the large Stokes shifts in $(\text{C}_4\text{N}_2\text{H}_{14}\text{Br})_4\text{SnBr}_6$ (215 nm) and $(\text{C}_4\text{N}_2\text{H}_{14}\text{I})_4\text{SnI}_6$ (210 nm)¹⁵ prevent the spectral overlap; in addition, the presence of large organic cations suppresses electronic coupling among $(\text{SnX}_6)^{4-}$ octahedra as shown by the nearly dispersionless valence and conduction bands [Fig. 2(a) and (c)]. Therefore, no significant resonant transfer of the excitation energy is expected (Fig. 4). The resulting immobile excitons in $(\text{C}_4\text{N}_2\text{H}_{14}\text{X})_4\text{SnX}_6$ (X = Br, I) have a low probability of interacting with the intrinsic defects, thereby leading to a high PLQE as observed in experiment.¹⁵ The immobility of excitons is important because the defect density in solution-grown hybrid halide perovskites is likely high as suggested by the significant absorption tail below the optical absorption edge in $(\text{C}_4\text{N}_2\text{H}_{14}\text{X})_4\text{SnX}_6$ (X = Br, I).¹⁵ The defect-related optical emission is absent from the PL spectra. The PL intensity in $(\text{C}_4\text{N}_2\text{H}_{14}\text{Br})_4\text{SnBr}_6$ displays linear dependence on the excitation power¹⁵ instead of a saturation behavior that is expected when the defects are filled by photo-excited electrons. This behavior indicates that the emission is due to excitons not defects.^{46,47} Direct optical excitation at the energies within the absorption tail (below the absorption edge) does not lead to any observable emission. Our calculated excitation and emission

Table 3 Excitation and emission energies of halogen-vacancy-bound excitons and Stoke shifts as well as the exciton binding energy at the halogen vacancies in $(\text{C}_4\text{N}_2\text{H}_{14}\text{Br})_4\text{SnBr}_6$, $(\text{C}_4\text{N}_2\text{H}_{14}\text{I})_4\text{SnI}_6$, and Cs_4PbBr_6 , calculated using hybrid PBE0 functionals

	Excitation energy (eV)	Emission energy (eV)	Stokes shift (eV)	Exciton trapping energy (eV)
$(\text{C}_4\text{N}_2\text{H}_{14}\text{Br})_4\text{SnBr}_6$	3.58	1.81	1.77	0.41
$(\text{C}_4\text{N}_2\text{H}_{14}\text{I})_4\text{SnI}_6$	3.11	1.65	1.46	0.22
Cs_4PbBr_6	3.32	2.53	0.79	0.59

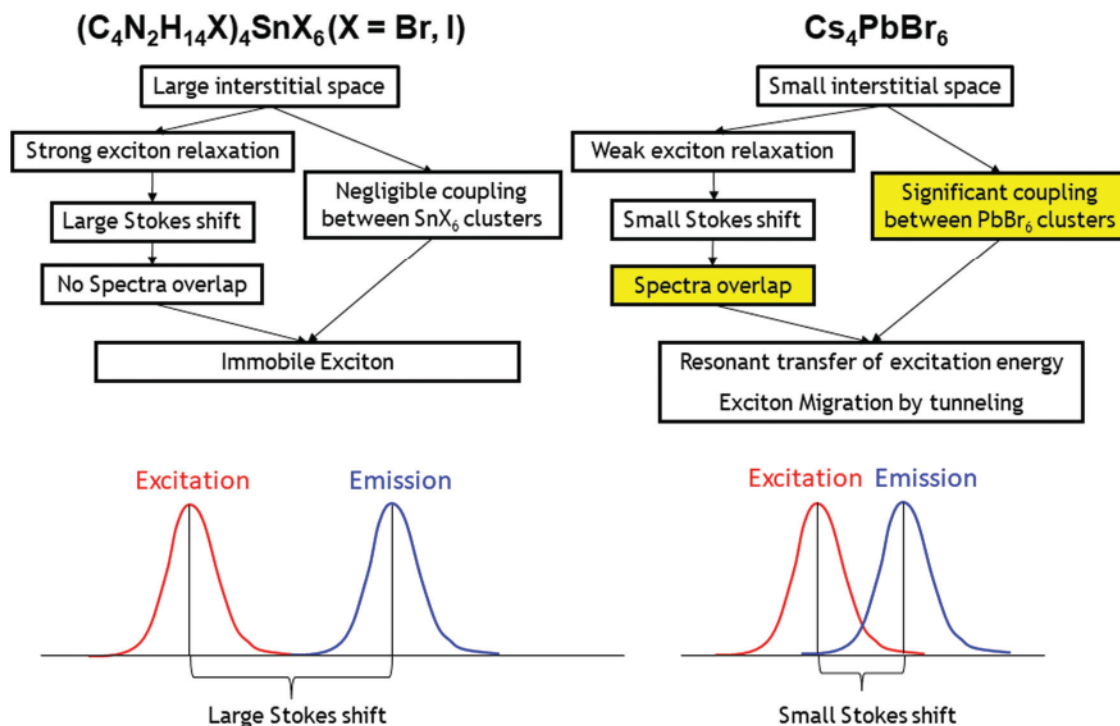


Fig. 4 Illustration of the mechanisms that lead to the immobile excitons in $(C_4N_2H_{14}X)_4SnX_6$ ($X = Br, I$) and the mobile excitons in Cs_4PbBr_6 . Excitons are deeply bound in all three compounds. However, the excitons in Cs_4PbBr_6 can migrate by tunneling.

due to bound excitons at halogen vacancies (Table 3) were not observed in experiment. These results suggest that the rate of nonradiative recombination at defects may be high, which suppresses the optical emission from excitons excited locally at defects. Therefore, suppressing exciton migration and exciton-defect interaction is essential to efficient luminescence, which highlights the importance of large organic cations that prevents the transport of excitation energy.

F. Green emission in Cs_4PbBr_6

We have explained the thermal quenching of the UV emission in Cs_4PbBr_6 above. Next, we discuss the origin of the frequently observed green emission (~ 520 nm or 2.39 eV) in Cs_4PbBr_6 . The calculated fundamental band gap (4.8 eV) and excitonic absorption energy (3.63 eV) are both substantially higher than the optical absorption edge (2.3–2.4 eV) in green-emitting Cs_4PbBr_6 , which suggest that the green emission is not due to the exciton emission in Cs_4PbBr_6 . The Br vacancy (V_{Br})³¹ and the Pb antisite defect [Pb_{Cs} (Pb occupying a Cs site)]³² have also been suggested to be the origin of green emission in Cs_4PbBr_6 . However, the calculated Stokes shift of 0.79 eV of the bound exciton at V_{Br}^+ (Table 3) is substantially larger than that observed in green-emitting Cs_4PbBr_6 (< 0.1 eV) [due to the strong excited-state structural relaxation (see Section S4 in ESI†)]; the calculated emission energy of the bound exciton at Pb_{Cs}^+ (0.99 eV) is too small to account for the green emission (2.3–2.4 eV). Therefore, our calculations do not support the V_{Br}^+ - or Pb_{Cs}^+ -induced green emission mechanism.

In fact, the experimentally observed onset of the optical absorption,^{23,26,28,31} excitation and the emission energies

(2.3–2.4 eV), the narrow emission band (15–24 nm),^{23–25,28,31} and the fast PL decay (a few to a few tens of ns)^{23–25,28,31} observed in green-emitting Cs_4PbBr_6 all agree well with those observed in $CsPbBr_3$.^{52,53} Several papers reported that the emission energy is slightly higher than the optical absorption edge,^{26,27,31} which is also consistent with the above-band-gap emission observed in bulk $CsPbBr_3$.^{52,53} A recent review of the experimental studies of Cs_4PbBr_6 supported the view that the green emission is due to $CsPbBr_3$ nanocrystals embedded in bulk Cs_4PbBr_6 .³³ We provide additional discussion on the experimental measurements on the band gap, the exciton binding energy, and the dependence of the PL intensity on excitation power in green-emitting Cs_4PbBr_6 in the ESI† (Section S5).

The above experimental and theoretical results suggest that the observed optical absorption (2.3–2.4 eV) and the subsequent green emission in Cs_4PbBr_6 is likely due to $CsPbBr_3$ inclusions trapped in Cs_4PbBr_6 . The small $CsPbBr_3$ inclusions serve as efficient luminescent centers in Cs_4PbBr_6 , which trap excitons due to the much smaller band gap of $CsPbBr_3$ than that of Cs_4PbBr_6 . The encapsulating Cs_4PbBr_6 may play the role of surface passivation for the $CsPbBr_3$ inclusions, which enhances the PLQE. The PLQE of the green-emitting Cs_4PbBr_6 was measured using sub-band-gap excitation energies below the excitonic absorption energy of Cs_4PbBr_6 ^{24,27,31} and, therefore, should be the PLQE of Cs_4PbBr_6 -encapsulated $CsPbBr_3$ (in analogy to core-shell structured quantum dots). A recent experimental study demonstrated the high PLQE of 97% in green-emitting Cs_4PbBr_6 and showed $CsPbBr_3$ nanocrystals embedded in Cs_4PbBr_6 based on high-resolution transmission electron microscopy.²⁹

IV. Summary and outlook

Hybrid DFT calculations have been performed to gain a fundamental understanding of the different photophysical properties of 0D hybrid organic–inorganic halides $(\text{C}_4\text{N}_2\text{H}_{14}\text{X})_4\text{SnX}_6$ ($\text{X} = \text{Br}, \text{I}$) and the inorganic metal halide Cs_4PbBr_6 . The calculated exciton excitation and emission energies agree very well with the experimental results. These 0D halides all have strongly bound excitons, which cannot be detrapped or dissociated at RT. As a result, the excitons in $(\text{C}_4\text{N}_2\text{H}_{14}\text{X})_4\text{SnX}_6$ ($\text{X} = \text{Br}, \text{I}$) are immobile. However, excitons can migrate in Cs_4PbBr_6 by tunneling enabled by the resonant transfer of excitation energy (Fig. 4). The relatively small Cs^+ cation in Cs_4PbBr_6 leads to electronic coupling between luminescent centers (PbBr_6 clusters) and spectral overlap between excitation and emission – the two conditions that enable the resonant energy transfer (exciton tunneling). The exciton migration in Cs_4PbBr_6 results in energy loss at the defects. Thus, these results explain the high PLQE in $(\text{C}_4\text{N}_2\text{H}_{14}\text{X})_4\text{SnX}_6$ and the strong thermal quenching of the UV emission in Cs_4PbBr_6 . The frequently observed green emission (~ 520 nm) in Cs_4PbBr_6 is not due to the exciton or defect-induced emission in Cs_4PbBr_6 but rather the result of exciton trapping and emission by CsPbBr_3 inclusions in bulk Cs_4PbBr_6 . We suggest that a large Stokes shift and the negligible electronic coupling between luminescent centers in 0D metal halides are important for suppressing exciton migration; thereby, enhancing the photoluminescence quantum efficiency. Although the all-inorganic halide Cs_4PbBr_6 is not emissive at RT, efficient luminescence may be found in 0D inorganic halides, which have more effective exciton traps such as Eu^{2+} , or in double perovskite halides, in which the distance between luminescent centers is long. These insights are useful for the future development of highly luminescent 0D metal halides as bright phosphors (for lighting) and scintillators (for radiation detection).

Conflicts of interest

There are no conflicts to declare.

Acknowledgements

We are grateful for the useful discussion with Yuntao Wu. The work at ORNL were supported by the U.S. Department of Energy, Office of Science, Basic Energy Sciences, Materials Sciences and Engineering Division (W. Ming and M.-H. Du) and the Chemical Sciences, Geosciences, and Biosciences Division (Y.-Z. Ma). D. Han and S. Chen were supported by the State Scholarship Fund in China and CC of ECNU. H. Shi was supported by the National Natural Science Foundation of China (NSFC) under Grant No. 11604007 and the start-up funding at Beihang University. B. Ma was supported by the Florida State University Energy and Materials Initiative and the National Science Foundation (DMR-1709116). B. Saparov was supported by the University of Oklahoma startup funds and by a grant from the Research Council of the University of Oklahoma Norman Campus.

References

- 1 B. Saparov and D. B. Mitzi, *Chem. Rev.*, 2016, **116**, 4558–4596.
- 2 M. A. Green, A. Ho-Baillie and H. J. Snaith, *Nat. Photonics*, 2014, **8**, 506–514.
- 3 J. Berry, T. Buonassisi, D. A. Egger, G. Hodes, L. Kronik, Y.-L. Loo, I. Lubomirsky, S. R. Marder, Y. Mastai, J. S. Miller, D. B. Mitzi, Y. Paz, A. M. Rappe, I. Riess, B. Rybtchinski, O. Stafsudd, V. Stevanovic, M. F. Toney, D. Zitoun, A. Kahn, D. Ginley and D. Cahen, *Adv. Mater.*, 2015, **27**, 5102–5112.
- 4 C. Zuo, H. J. Bolink, H. Han, J. Huang, D. Cahen and L. Ding, *Adv. Sci.*, 2016, **3**, 1500324.
- 5 https://www.nrel.gov/ncpv/images/efficiency_chart.jpg.
- 6 S. A. Veldhuis, P. P. Boix, N. Yantara, M. Li, T. C. Sum, N. Mathews and S. G. Mhaisalkar, *Adv. Mater.*, 2016, **28**, 6804–6834.
- 7 P. Li, Y. Chen, T. Yang, Z. Wang, H. Lin, Y. Xu, L. Li, H. Mu, B. N. Shivananju, Y. Zhang, Q. Zhang, A. Pan, S. Li, D. Tang, B. Jia, H. Zhang and Q. Bao, *ACS Appl. Mater. Interfaces*, 2017, **9**, 12759–12765.
- 8 H. Wei, Y. Fang, P. Mulligan, W. Chuirazzi, H.-H. Fang, C. Wang, B. R. Ecker, Y. Gao, M. A. Loi, L. Cao and J. Huang, *Nat. Photonics*, 2016, **10**, 333–339.
- 9 E. R. Dohner, E. T. Hoke and H. I. Karunadasa, *J. Am. Chem. Soc.*, 2014, **136**, 1718–1721.
- 10 E. R. Dohner, A. Jaffe, L. R. Bradshaw and H. I. Karunadasa, *J. Am. Chem. Soc.*, 2014, **136**, 13154–13157.
- 11 T. Hu, M. D. Smith, E. R. Dohner, M.-J. Sher, X. Wu, M. T. Trinh, A. Fisher, J. Corbett, X. Y. Zhu, H. I. Karunadasa and A. M. Lindenberg, *J. Phys. Lett.*, 2016, **7**, 2258–2263.
- 12 Z. Yuan, Y. Shu, Y. Tian, Y. Xin and B. Ma, *Chem. Commun.*, 2015, **51**, 16385–16388.
- 13 Z. Yuan, Y. Shu, Y. Xin and B. Ma, *Chem. Commun.*, 2016, **52**, 3887–3890.
- 14 Z. Yuan, C. Zhou, Y. Tian, Y. Shu, J. Messier, J. C. Wang, L. J. van de Burgt, K. Kountouriotis, Y. Xin, E. Holt, K. Schanze, R. Clark, T. Siegrist and B. Ma, *Nat. Commun.*, 2017, **8**, 14051.
- 15 C. Zhou, H. Lin, Y. Tian, Z. Yuan, R. J. Clark, B. Chen, B. van de Burgt, J. C. Wang, Y. Zhou, K. Hanson, Q. Meisner, J. Neu, T. Besara, T. Siegrist, E. Lambers, P. I. Djurovich and B. Ma, *Chem. Sci.*, 2018, **9**, 586–593.
- 16 Q. Dong, Y. Fang, Y. Shao, P. Mulligan, J. Qiu, L. Cao and J. Huang, *Science*, 2015, **347**, 967–970.
- 17 S. D. Stranks, G. E. Eperon, G. Grancini, C. Menelaou, M. J. P. Alcocer, T. Leijtens, L. M. Herz, A. Petrozza and H. J. Snaith, *Science*, 2013, **342**, 341–344.
- 18 G. Xing, N. Mathews, S. Sun, S. S. Lim, Y. M. Lam, M. Grätzel, S. Mhaisalkar and T. C. Sum, *Science*, 2013, **342**, 344–347.
- 19 D. Shi, V. Adinolfi, R. Comin, M. J. Yuan, E. Alarousu, A. Buin, Y. Chen, S. Hoogland, A. Rothenberger, K. Katsiev, Y. Losovyj, X. Zhang, P. A. Dowben, O. F. Mohammed, E. H. Sargent and O. M. Bakr, *Science*, 2015, **347**, 519–522.
- 20 H. Lin, C. Zhou, Y. Tian, T. Siegrist and B. Ma, *ACS Energy Lett.*, 2017, **54–62**, DOI: 10.1021/acsenerylett.7b00926.

- 21 C. Zhou, H. Lin, H. Shi, Y. Tian, C. Pak, M. Shatruk, Y. Zhou, P. Djurovich, M. Du and B. Ma, *Angew. Chem., Int. Ed.*, 2018, 57, 1021–1024.
- 22 W. Liu, K. Zhu, S. J. Teat, G. Dey, Z. Shen, L. Wang, D. M. O'Carroll and J. Li, *J. Am. Chem. Soc.*, 2017, 139, 9281–9290.
- 23 M. I. Saidaminov, J. Almutlaq, S. Sarmah, I. Dursun, A. A. Zhumeikenov, R. Begum, J. Pan, N. Cho, O. F. Mohammed and O. M. Bakr, *ACS Energy Lett.*, 2016, 1, 840–845.
- 24 Y. Zhang, M. I. Saidaminov, I. Dursun, H. Yang, B. Murali, E. Alarousu, E. Yengel, B. A. Alshankiti, O. M. Bakr and O. F. Mohammed, *J. Phys. Chem. Lett.*, 2017, 8, 961–965.
- 25 S. Seth and A. Samanta, *J. Phys. Chem. Lett.*, 2017, 8, 4461–4467.
- 26 J.-H. Cha, J. H. Han, W. Yin, C. Park, Y. Park, T. K. Ahn, J. H. Cho and D.-Y. Jung, *J. Phys. Chem. Lett.*, 2017, 8, 565–570.
- 27 H. Zhang, Q. Liao, Y. Wu, J. Chen, Q. Gao and H. Fu, *Phys. Chem. Chem. Phys.*, 2017, 19, 29092.
- 28 D. Chen, Z. Wan, X. Chen, Y. Yuan and J. Zhong, *J. Mater. Chem. C*, 2016, 4, 10646–10653.
- 29 X. Chen, F. Zhang, Y. Ge, L. Shi, S. Huang, J. Tang, Z. Lv, L. Zhang, B. Zou and H. Zhong, *Adv. Funct. Mater.*, 2018, 28, 1706567.
- 30 Q. A. Akkerman, S. Park, E. Radicchi, F. Nunzi, E. Mosconi, F. De Angelis, R. Brescia, P. Rastogi, M. Prato and L. Manna, *Nano Lett.*, 2017, 17, 1924–1930.
- 31 M. De Bastiani, I. Dursun, Y. Zhang, B. A. Alshankiti, X.-H. Miao, J. Yin, E. Yengel, E. Alarousu, B. Tureddi, J. M. Almutlaq, M. I. Saidaminov, S. Mitra, I. Gereige, A. AlSaggaf, Y. Zhu, Y. Han, I. S. Roqan, J.-L. Bredas, O. F. Mohammed and O. M. Bakr, *Chem. Mater.*, 2017, 29, 7108–7113.
- 32 J. Yin, Y. Zhang, A. Bruno, C. Soci, O. M. Bakr, J.-L. Brédas and O. F. Mohammed, *ACS Energy Lett.*, 2017, 2805–2811, DOI: 10.1021/acsenerylett.7b01026.
- 33 Q. A. Akkerman, A. L. Abdelhady and L. Manna, *J. Phys. Chem. Lett.*, 2018, 2326–2337, DOI: 10.1021/acs.jpclett.8b00572.
- 34 M. Nikl, E. Mihokova, K. Nitsch, F. Somma, C. Giampaolo, G. P. Pazzi, P. Fabeni and S. Zazubovich, *Chem. Phys. Lett.*, 1999, 306, 280–284.
- 35 J. P. Perdew, K. Burke and M. Ernzerhof, *Phys. Rev. Lett.*, 1996, 77, 3865.
- 36 J. P. Perdew, M. Ernzerhof and K. Burke, *J. Chem. Phys.*, 1996, 105, 9982–9985.
- 37 C. Zhou, H. Lin, H. Shi, Y. Tian, C. Pak, M. Shatruk, Y. Zhou, P. Djurovich, M.-H. Du and B. Ma, *Angew. Chem., Int. Ed.*, 2018, 57, 1021.
- 38 J. Even, L. Pedesseau, J.-M. Jancu and C. Katan, *J. Phys. Chem. Lett.*, 2013, 4, 2999–3005.
- 39 J. Yin, P. Maity, M. De Bastiani, I. Dursun, O. M. Bakr, J.-L. Brédas and O. F. Mohammed, *Sci. Adv.*, 2017, 3, e1701793.
- 40 M.-H. Du and D. J. Singh, *Phys. Rev. B: Condens. Matter Mater. Phys.*, 2010, 81, 144114.
- 41 M.-H. Du and D. J. Singh, *Phys. Rev. B: Condens. Matter Mater. Phys.*, 2010, 82, 045203.
- 42 M. H. Du, *J. Mater. Chem. A*, 2014, 2, 9091–9098.
- 43 B. Kang and K. Biswas, *J. Phys. Chem. Lett.*, 2018, 9, 830–836.
- 44 K. Biswas and M. H. Du, *Phys. Rev. B: Condens. Matter Mater. Phys.*, 2012, 86, 014102.
- 45 S. Kondo, K. Amaya and T. Saito, *J. Phys.: Condens. Matter*, 2002, 14, 2093.
- 46 W. Ming, S. Chen and M.-H. Du, *J. Mater. Chem. A*, 2016, 4, 16975–16981.
- 47 A. Walsh, D. O. Scanlon, S. Y. Chen, X. G. Gong and S. H. Wei, *Angew. Chem., Int. Ed.*, 2015, 54, 1791–1794.
- 48 M. H. Du, *J. Phys. Chem. Lett.*, 2015, 6, 1461–1466.
- 49 H. Shi and M.-H. Du, *Phys. Rev. B: Condens. Matter Mater. Phys.*, 2014, 90, 174103.
- 50 G. Blasse and B. C. Grabmaier, *Luminescent Materials*, Springer-Verlag, Berlin, Heidelberg, 1994.
- 51 D. L. Dexter, *J. Chem. Phys.*, 1953, 21, 836–850.
- 52 M. Sebastian, J. A. Peters, C. C. Stoumpos, J. Im, S. S. Kostina, Z. Liu, M. G. Kanatzidis, A. J. Freeman and B. W. Wessels, *Phys. Rev. B: Condens. Matter Mater. Phys.*, 2015, 92, 235210.
- 53 Q. A. Akkerman, M. Gandini, F. Di Stasio, P. Rastogi, F. Palazon, G. Bertoni, J. M. Ball, M. Prato, A. Petrozza and L. Manna, *Nat. Energy*, 2016, 2, 16194.